Mater.Phys.Mech.1 (2000) 83-97

InO_X THIN FILMS, CANDIDATES FOR NOVEL CHEMICAL AND OPTOELECTRONIC APPLICATIONS

G. Kiriakidis, N. Katsarakis, M. Bender, E. Gagaoudakis and V. Cimalla

Institute of Electronic Structure and Laser (IESL), Foundation for Research and Technology-Hellas (FO.R.T.H), P.O. Box 1527, Heraklion 711 10, Greece

Received: June 7,2000

Abstract. The potentials of InO_x microcrystalline thin films for novel chemical and optoelectronic applications are investigated. In particular, these films are candidates for gas sensor applications due to their sensitivity to reactive gas environments such as ozone. This sensitivity is recorded as the result of the variation of the film conductivity level up to six orders of magnitude, which is attributed to the formation of oxygen vacancies. The microcrystalline nature of the films is investigated by X-ray Diffraction (XRD) and Transmission Electron Microscopy (TEM) while film surface characteristics are revealed by Atomic Force Microscopy (AFM). Depth profiling is examined by Auger Electron Spectroscopy (AES) while the stoichiometry of the films is determined by Energy Dispersive X-Ray analysis (EDX). Finally, the photorefractive properties of InO_x films as well as their potential for the fabrication of optical gratings for novel telecom and waveguide applications are discussed.

1. INTRODUCTION

Indium oxide (InO_x) is a very important material for microelectronic applications. It is an insulator in its stoichiometric form, whereas in its non-stoichiometric form it behaves as a highly conducting semiconductor with a wide optical band-gap (~3.7 eV), providing high transparency in the visible light range and high reflectivity in the infrared (IR) light range. This unique combination of electrical and optical properties has led numerous researchers to a thorough investigation of the growth and characterization of thin semiconducting indium oxide films because of their obvious application in optoelectronic devices, such as solar cells, diffusion barriers in Al/InO_x/Si stuctures and flat panel displays and as a photosensitive overlayer in telecom and sensor waveguide applications. Several deposition techniques have been employed for the growth of polycrystalline indium oxide films, such as dc and rf sputtering [1-3], reactive evaporation [4-9], evaporation of metallic indium and subsequent oxidation [10,11], chemical vapour deposition [12], spray pyrolysis [13,14] and laser ablation [15]. In the majority of the reported studies, InO_x films have been prepared by reactive sputtering and evaporation, since these techniques seem to give the best results and combine reproducibility and low cost. Of these two methods, the sputtering process has the advantage of producing films that are mechanically stable and with good substrate adhesion.

Over the last few years, it has been shown by Fritzsche et al. [16-19] that the stoichiometry and electrical properties of amorphous InO_x films (with a thickness below 80 nm) prepared by dc reactive sputtering can dramatically change under exposure to ultraviolet (UV) light ($h\nu \geq 3.5$ eV) in vacuum or in an inert gas atmosphere. It has been demonstrated that the conductivity can be increased by about six orders of magnitude by exposing the film to ultraviolet (UV) light in vacuum, while by subsequently exposing the same film to an oxidizing atmosphere, the film reverts to the insulating state. In a previous article [20] of our group, it has been demonstrated that these large reversible conductivity changes produced by UV photoreduction and oxidation are not limited to amorphous InO_x but are also characteristic of microcrystalline InO_x films of larger thickness (well above 80 nm). The mechanism responsible for these changes in conductivity is believed to be related to the UV-induced production of oxygen vacancies that act as doubly charged donors resulting in a degenerate electron gas in the conduction band [21]. Oxygen vacancies are equivalent to oxygen deficiency with respect to stoichiometric composition.

Corresponding author: G. Kiriakidis, e-mail: kiriakid@iesl.forth.gr

© 2000 Advanced Study Center Co. Ltd.

By means of transmission electron microscopy and electron diffraction it has been found that the structure of the films, i.e. the crystallinity and the microstucture, are greatly dependent on the substrate temperature as well as on the film thickness [5]. An amorphous to polycrystalline transition occurs by increasing substrate temperature and film thickness. Annealing of the amorphous indium oxide films at 200 °C gives also rise to the transition [2,22], while further annealing of the polycrystalline phase at temperatures higher than 400 °C may cause a change in the microstructure of the films (both in size and shape of the crystallites) [23]. The oxygen partial pressure during deposition affects not only the electrical but also the optical and structural properties of the films [6]. Thus by increasing the oxygen partial pressure, an increase in the direct optical band gap value from 3.67 to 3.92 eV, well known as Burstein-Moss shift, and a progressive crystal growth resulting in an increase of the grain size of the films have been observed. Although extensive work has been published about the electrical, optical and structural properties of InO_x films, there have so far been only a few studies concerning chemical characterization of these films [24-31].

In this article previous work on the photorefractive and oxidation studies of thin InO_x films is extended with in-depth structural, optical and chemical studies. The potential of InO_x thin films for gas sensor and photorefractive applications is demonstrated. Structural analysis of the samples and topological analysis of the film surfaces have been performed by X-ray diffraction (XRD) and atomic force microscopy (AFM), while the surface and depth composition of films has been examined by Auger electron spectrosopy (AES) combined with depth profile analysis. It is demonstrated that the microcrystalline InO_x films prepared by dc reactive sputtering exhibit good in-depth uniformity regardless of their film thickness in the range of 120-1600 nm. Quantitative Auger and energy dispersive X-Ray (EDX) analyses have been applied to determine the stoichiometry of InO_x films. An oxygen deficiency of 2-5% has been observed with respect to the stoichiometric composition. The effect of film thickness and oxygen content in the sputtering gas on the stoichiometry has been examined. Both AES and EDX analyses have confirmed that the stoichiometry is invariant for these parameters.

Finally, the photorefractive properties of these films have been investigated [15, 32-34] and optical gratings (~0.65 nm) have been produced utilizing two coherent 325 nm beams and recording conductivity related holographic dynamics. By utilizing a 193 nm excimer laser source, permanent recording charcteristics have been obtained giving rise to a new range of potential applicatons for InO_x films as photosensitive overlayer in telecom and sensor waveguides.

2. EXPERIMENTAL DETAILS

Microcrystalline indium oxide (InO_x) thin films were deposited on Corning glass substrates by dc magnetron sputtering. They were grown in a mixture of argon-oxygen plasma at total pressure of $8 \cdot 10^{-3}$ mbar using a 99.999% pure indium target (the oxygen volume fractions in the argon-oxygen plasma used were F=0.4, 0.5, 0.6, 0.7, 0.8, 0.9 and 1.0). The thickness of the films was in the range of 120-1600 nm. All details of the preparation of the films are provided elsewhere [20]. Photoreduction and oxidation experiments were carried out on the as-deposited microcrystalline InO_x films. The apparatus used was a glass chamber pumped down by a rotary pump. A miniature short-wave pencil mercury lamp from Edmund Scientific Co. with an average intensity of 4 mW/cm^2 at λ=254 nm, which is normally used for wavelength calibration of spectrometers, served as an ultraviolet (UV) light source at a distance of 3 cm from the samples. For photoreduction the samples were exposed directly to UV light in vacuum. Oxidation was carried out in the same chamber with the samples exposed to ozone produced by the UV light source in 600 Torr of O_2, while the samples were shielded from direct exposure to UV light. A field of about 1 V/cm was applied to the samples and the current was measured with a Keithley 616 electrometer. Optical measurements of both transmission and absorption were carried out on InO_x films deposited onto Desag glass substrates with an absorption edge at 330 nm, using a Perkin-Elmer VIS/UV spectrometer.

The deposited films were analyzed in an XRD system using a CuK_α source (λ=1.54506 Å) in the $\theta/2\theta$ geometry. The surface of the films was investigated by atomic force microscopy in air, using a Digital Instruments Nanoscope IIa in both tapping and contact mode with Si_3N_4 or Si tips respectively.

For the transmission electron microscopy (TEM) and electron diffraction studies, InO_x films with a thickness of about 100 nm were deposited onto freshly cleaved NaCl single crystals. After the deposition, the films were removed from the NaCl substrates by dissolving the salt in distilled water and were mounted onto copper grids. The samples were examined using a JEOL Temscan 100 CX microscope operated at 100 kV.

Surface and depth composition analyses of the films were carried out in an ion- and turbo- pumped stainless steel UHV chamber with facilities for Auger analysis. The chamber was pumped to a base pressure of $1 \cdot 10^{-10}$ mbar after mild baking and samples were exchanged via a load lock chamber. The primary elec-

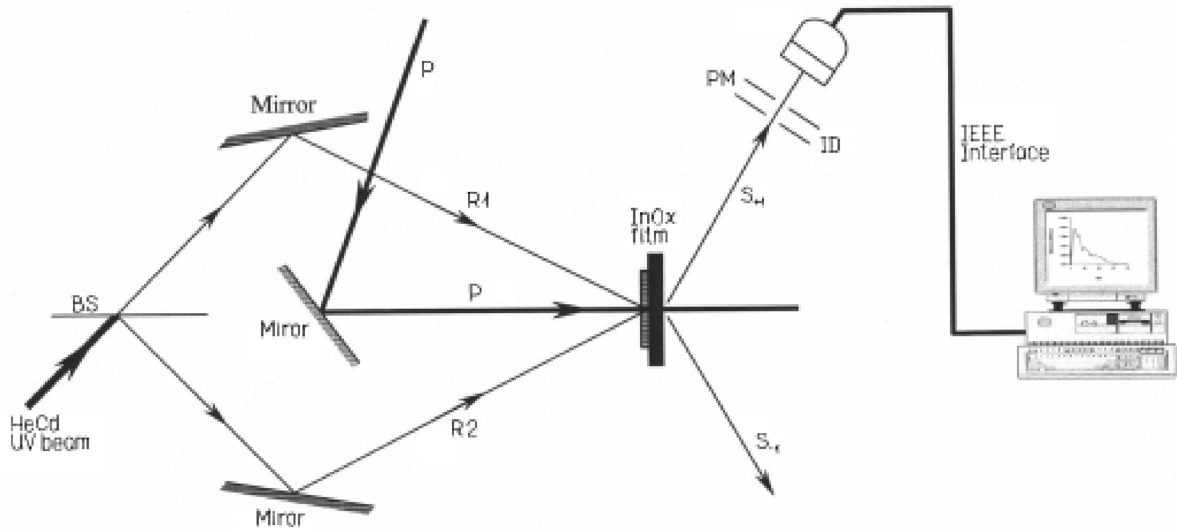

Fig. 1. Schematic representation of the experimental set-up R_1, R_2: recording beams at 325 nm, P: HeNe probe beam at 632.8 nm, $S_{\pm 1}$: diffracted HeNe beams, BS: beamsplitter, PM: powermeter-head, ID: iris diaphragm.

tron beam energy and current were 2.5 keV and 5 μA respectively. The Auger signal, $dN(E)/dE$, was measured with a lock-in amplifier using a time constant of 750 ms and a modulation voltage of 5 V peak-to-peak. An argon ion beam with energy of 1 keV was employed for depth profiling analysis. This beam spot was rastered over an area of 4·4 mm^2. Data acquisition, storage and processing were accomplished using a computer program for sputter profiling analysis written in LABVIEW™.

To examine the average stoichiometry of the films, an energy dispersive x-ray analysis (EDX) system attached to a scanning electron microscope (Philips SEM 535 with EDAX equipment) was used. Quantitative analysis with standards was carried out for InO_x films deposited on silicon substrates, which were produced with various mixtures of oxygen in argon (F = 0.4, 0.5, 0.6, 0.8 and 1.0). As standards, indium oxide grade 1 powder (purity of 99.995%) supplied by the Johnson Matthey Company was employed.

The set-up for the photorefractive studies is shown schematically in Fig.1. The beam of a HeCd laser emitting at λ=325 nm was divided in two mutually coherent beams, by means of a dielectric beam splitter. The two beams R_1 and R_2, with intensities of 300 mW/cm^2 each, were subsequently directed onto the sample, forming an intensity interference pattern. Numerous recordings at various fringe spacing values (Λ) have been studied. An HeNe laser beam was used to monitor the recording of the holographic grating. The 5.7 mW HeNe probe beam, P, was incident normally onto the surface of the film. Two scattered beams, $S_{\pm 1}$, of equal intensity were observed corresponding to the ±1 diffraction orders of the recorded sinusoidal grating. By using an optical power meter and a storage oscilloscope, one of the diffracted beams was monitored, in order to investigate the temporal characteristics of the recorded gratings.

Permanent holographic recording in sputtered InO_x thin films has also been recorded utilizing UV radiation at 193 nm by an ArF excimer laser. The photosensitivity of the films was investigated by exposing the samples to UV radiation with coherent pulses of 23 ns duration (FWHM) and beam energy of 100 mJ per pulse.

3. RESULTS

Photoreduction and oxidation. The conductivity of the as-deposited films was of the order of 10^{-4}–10^{-3} $\Omega^{-1}cm^{-1}$ and increased up to the order of 10^{1}–10^{2} $\Omega^{-1}cm^{-1}$ by exposure to ultraviolet (UV) light in vacuum. Fig. 2 shows very clearly this large change of conductivity for two films with thickness 240 and 210 nm, deposited with F=0.5 and 1.0 respectively. In Fig. 2, the conductivity of the films increased up to a saturation value by direct exposure to UV light. This is an induced change in dark conductivity by UV-light because the conductivity values remained constant when the UV light was turned off. Following the UV exposure, the same films were exposed to an oxidizing atmosphere by introducing 600 Torr of oxygen into the chamber. Under this exposure, the films were effectively reoxidized and their conductivity decreased by about six orders of magnitude to its as-deposited level. The processes of photoreduction and oxidation are fully reversible. The photoreduction and oxidation cycles were repeated many times and the conductivity regained the high saturation values of the same level, as shown in Fig. 2.

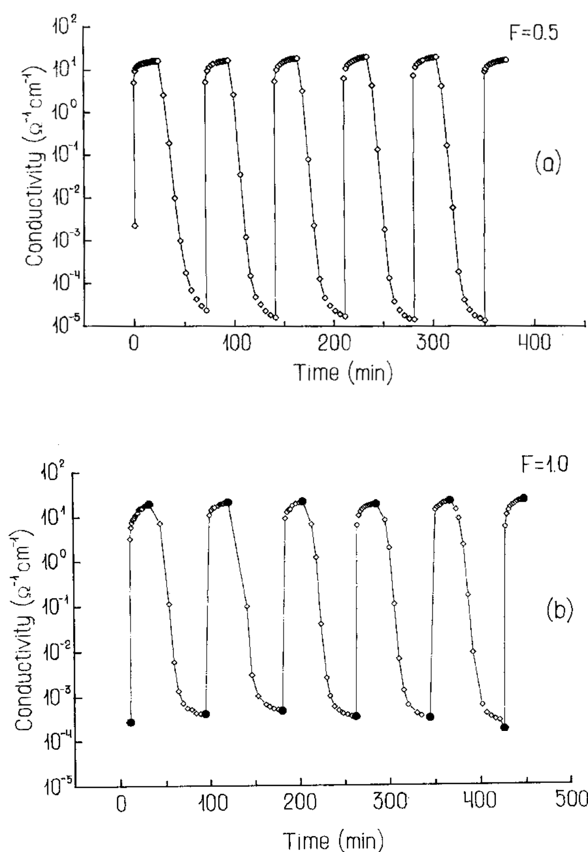

Fig. 2. (a)-(b). Photoreduction and oxidation of 240 and 210 nm thick as-deposited microcrystalline InO_x films produced in a plasma having an oxygen fraction of (a) F=0.5 and (b) F=1.0, respectively.

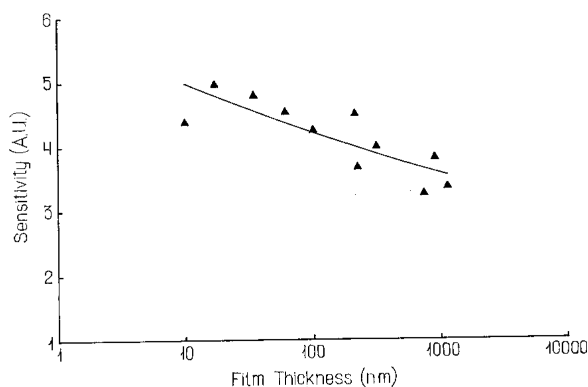

Fig. 3. Dependence of indium oxide film thickness on sensitivity to ozone.

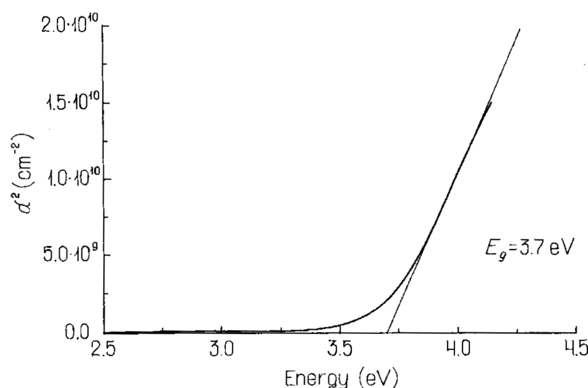

Fig. 4. a^2 vs $h\nu$ plot of as-deposited microcrystalline InO_x films.

Fig.3 shows the dependence of the ozone sensitivity on the thickness of the InO_x films. The sensitivity is defined as the difference in conductivities between the two states expressed in orders of magnitude. It can be seen that the sensitivity decreases with increasing film thickness from about 5 for very thin films with thicknesses around 10-20 nm to below 3.5 for InO_x films with thicknesses more than 1000 nm.

The as-deposited microcrystalline InO_x films were found to be highly transparent in the visible light region, as seen in Fig.4. A direct optical energy gap E_g=3.70±0.05 eV was determined for these films from optical absorption measurements [20]. The optical energy gap of all films was essentially the same for oxygen contents between F=0.5 and 1.0 in the sputtering gas.

Structural characterization of the InO_x films. All the deposited films but especially the thinnest, with a thickness of 10 nm, showed some diffraction peaks. Peaks belonging to the cubic structure of In_2O_3 could only be identified, giving evidence for the existence of single phase. From the XRD data the lattice constant was calculated. The lattice constant varies between 10.378 Å and 10.174 Å and decreases with increasing film thickness. The value of the lattice constant is in accordance with the literature value of 10.118 Å for the structure of stoichiometric indium oxide. This reveals that the films under discussion in this work are close to stoichiometric In_2O_3. From the FWHM of the diffraction line peaks the crystallite size was calculated using Scherrer's formula [20]. The crystallite sizes were found to be in the range of 100 to 150 Å almost independent from the film thickness. Therefore, it can be concluded, that the topology of the film is according to Zone 1 of Thorntons Zone-Structure-Model [35]. The films are consisting of small grains that are separated by grain boundaries. There are no indications for columnar grain growth under the deposition conditions chosen in this work.

The surface of the films was investigated by atomic force microscopy in air, using a Digital Instruments Nanoscope IIa in both tapping and contact mode using Si_3N_4 and Si tips respectively. Several AFM images of different scales from (0.5·0.5) to (10·10) μm^2 were taken for each sample to estimate surface roughness and grain size in dependence on different process conditions. The evolution of grain size and surface roughness rms versus deposition time is shown in Fig.5.

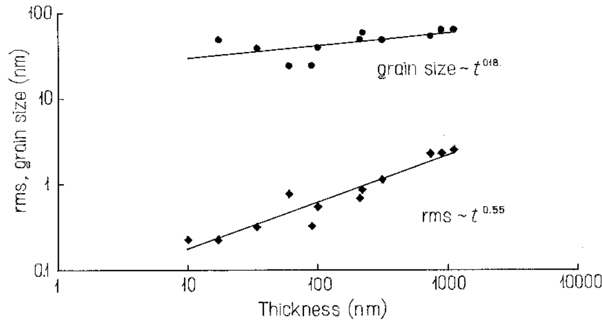

Fig. 5. Relation between grain size respectivelly surface roughness and film thickness.

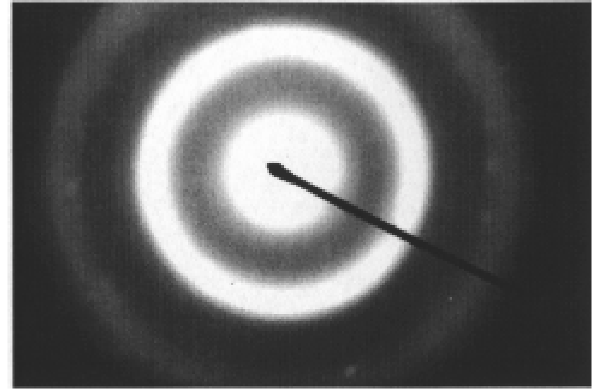

a)

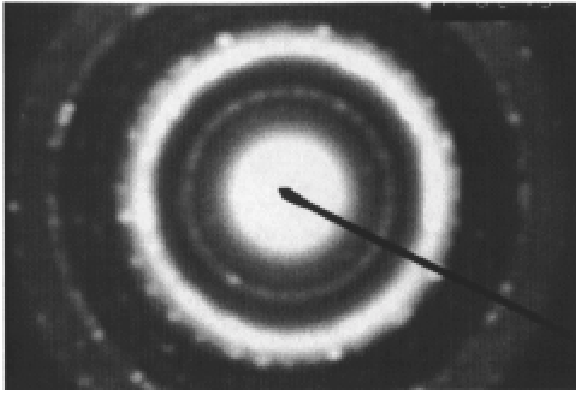

b)

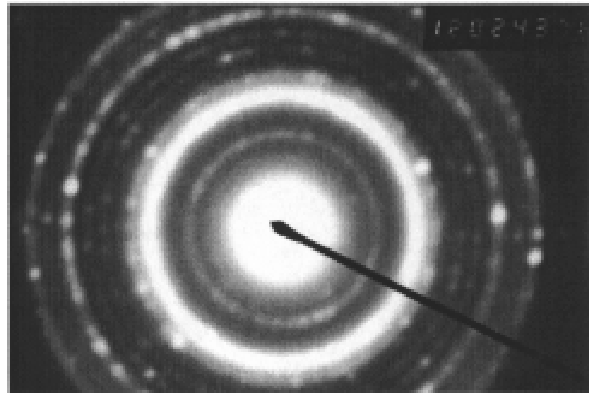

c)

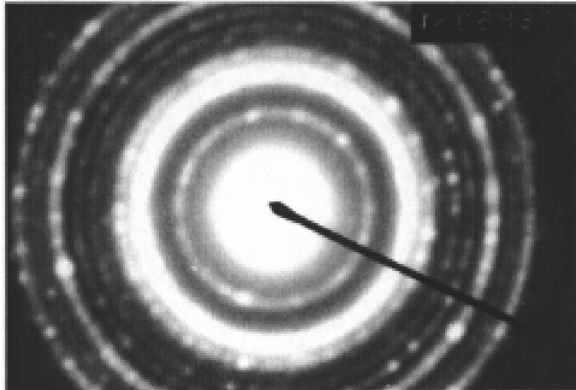

d)

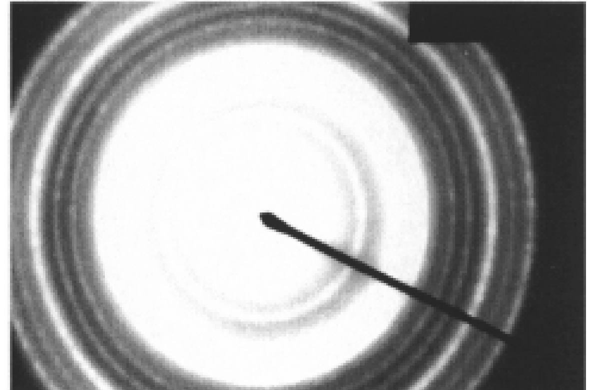

e)

Fig. 6. (a)–(e). Electron diffraction patterns of the same selected area of an InO_x film with thickness of about 100 nm as a function of the film exposure time to the focused electron beam. The initial mainly amorphous phase, (a), is transformed, (b)–(d), to a phase typical of a microcrystalline In_3O_2 film, (e), during *in-situ* recrystallization caused by the electron beam.

TEM studies carried out on InO_x films with a thickness of about 100 nm showed that an electron beam induced recrystallization mechanism takes place *in situ* in these films. Fig.6 shows a sequence of electron diffraction patterns produced from the same selected area of an InO_x film by increasing the time of film exposure to the focused electron beam. As seen in Fig.6(a), the diffraction pattern of the film initially consisted of diffuse rings with only a few crystallites embedded in the uniform matrix indicating mainly an amorphous phase with a trace of crystalline InO_x. This is due to the small thickness of the film. Usually, InO_x films deposited by dc reactive magnetron sputtering at room temperature in a mixture of argon-oxygen plasma exhibit a microcrystalline structure in their as-deposited state when they have a thickness above about 100 nm. The films used for TEM studies in the present work had a thickness $d \leq 100$ nm, being therefore at the limit between microcrystalline and amorphous phase. Thicker films have also been produced for TEM observations, however, they proved to be electron-impenetrable in this particular TEM system operated at 100 kV. Longer exposure of the film of Fig.6 (a) to the electron beam led to a diffraction pattern of Fig.6 (b). It is clear in

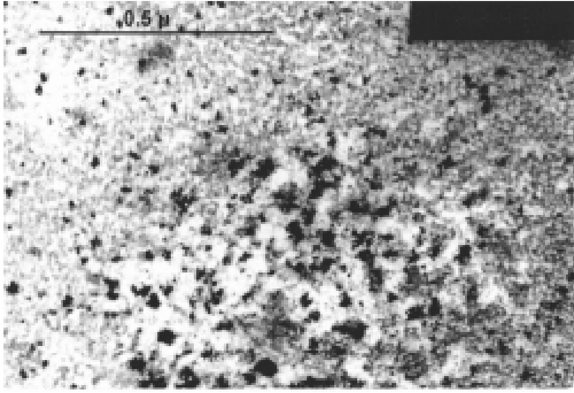

Fig. 7. Bright-field electron micrograph with magnification 66.000 of the InO_x film in Fig.6 after crystallization occured.

this figure that the crystallites embedded in the amorphous phase are now numerous and slightly larger, indicating a mixture of the amorphous and the microcrystalline phase. The fraction of the microcrystalline phase increased, while the fraction of the amorphous phase decreased, by extending the exposure time, as seen in Fig.6 (c). The diffraction pattern is now entirely composed of crystallites, which are so many that the diffraction pattern starts to form sharp rings ascribed to the In_2O_3 cubic structure. A further increase in the sharpness of the rings can be seen in Fig.6 (d). Finally, in Fig.6 (e), the sharp diffraction rings observed indicate that the initially mainly amorphous phase crystallized around the already present crystallites. This diffraction pattern is typical of a microcrystalline In_2O_3 film. These results are very interesting from the point of view that one can see very simply the transformation from the amorphous to the microcrystalline phase in one and the same film without involving any conventional post-deposition heat treatment. Fig.7 shows the corresponding bright-field electron micrograph with magnification 66.000 of the InO_x film after crystallization occurred. This micrograph exhibits a grainy structure which consists of many small grains of relatively uniform size forming a morphologically homogeneous film. However, two different regions can be easily recognized in this micrograph. The lower part of the micrograph corresponds to an area of the film exposed for longer time to the focused electron beam than the area shown at the upper part of the micrograph. As a result, a crystal growth appears in this area. This is a clear indication that the electron beam causes annealing of the film.

The lattice spacings d_{hkl} were calculated from the diffraction relationship:

$$d_{hkl} = \lambda L \frac{2}{D}, \qquad (1)$$

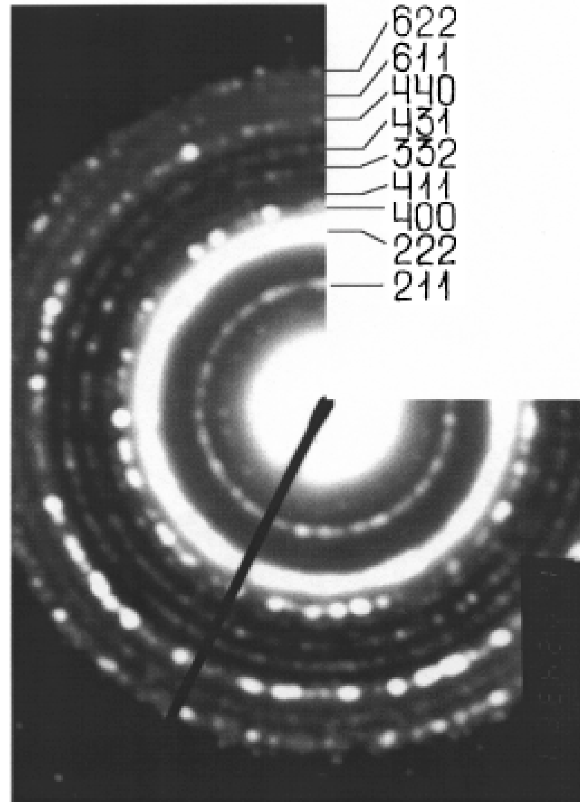

Fig. 8. Identification of the crystallographic planes corresponding to the observed diffraction rings in the electron diffraction pattern of the InO_x film in Fig. 6 after crystallization occured.

where λ is the de Broglie wavelength which can be calculated from the acceleration voltage after applying the relativistic correction, L is the distance between the sample and the photographic film, known as the camera length, and D is the diameter of the diffraction rings. To eliminate uncertainties in the acceleration voltage and camera length, a standard thallium chloride (TlCl) crystal was used as a reference for the diffraction measurements. From the most clearly visible diffraction ring in the diffraction pattern of TlCl corresponding to the (110) plane with a lattice spacing d_{110}=2.717Å·mm according to the ASTM diffraction data card 06-0486, the quantity $\lambda \cdot L$ (L in mm and λ in Å) was determined by measuring the diameter D of the ring, and it was found to be $\lambda \cdot L$=111.4 Å·mm. Subsequently, this value was used to calculate the lattice spacings of the InO_x film by measuring the diameter D of the diffraction rings in the diffraction pattern and using the Eq. 1. In this case, the relativistic correction was not necessary to be used, since the diffraction patterns of the standard TlCl crystal and the InO_x film were produced under the same experimental conditions. The lattice spacings d_{hkl} calculated for the InO_x are listed in the Table 1 together with the corresponding d_{hkl} values of the standard In_2O_3 powder provided in the ASTM diffraction data card 6-0416, for comparison. In Fig.8

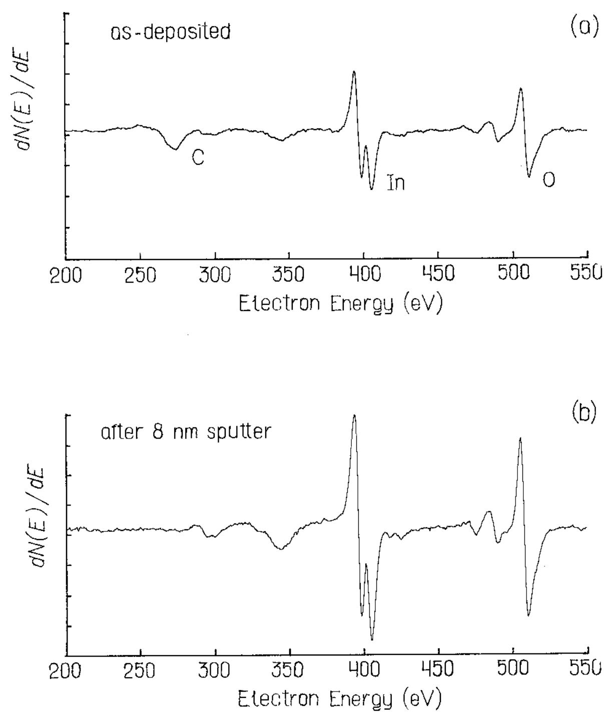

Fig. 9 (a)–(b). Typical Auger spectrum of a microcrystalline InO_x film for (a) the as-deposited state and (b) after 8 nm sputtering.

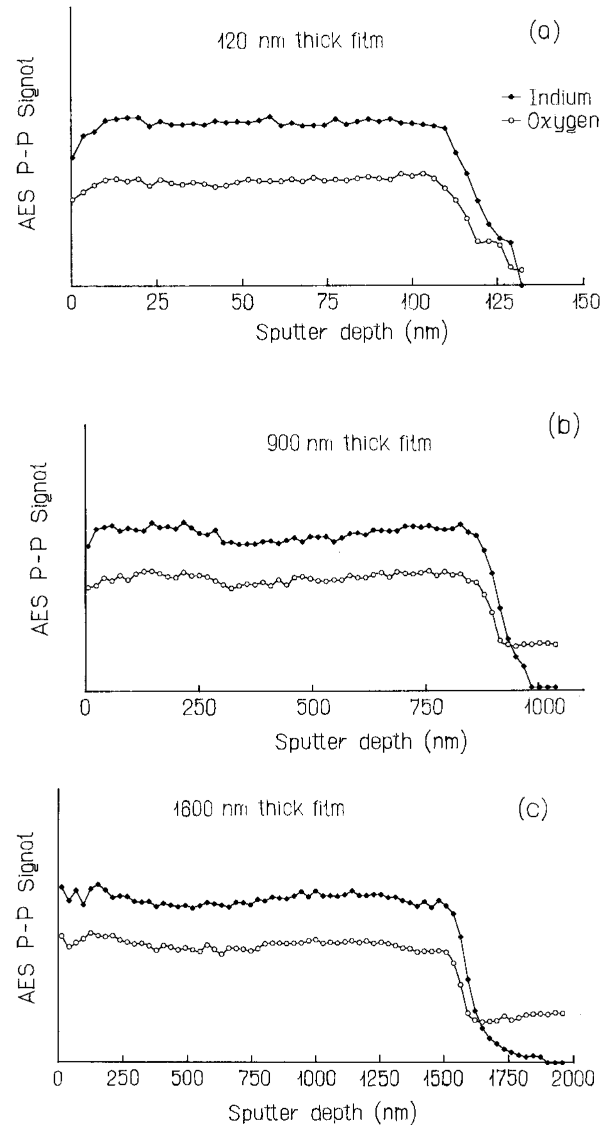

Fig. 10 (a)–(c). Auger depth profiles of (a) 120 nm, (b) 900 nm and (c) 1600 nm thick microcrystalline InO_x films.

the crystallographic planes corresponding to the observed diffraction rings are identified.

Chemical characterization of the films. A typical Auger spectrum of a microcrystalline InO_x film is shown in Fig. 9. The indium doublet which corresponds to MNN transitions appears at energies of 400 and 406 eV, while the oxygen peak which corresponds to KLL transitions appears at the energy of 511 eV. These energy values are in good agreement with those previously reported [36] (404, 410 and 510 eV, correspondingly). As seen from Fig. 9a, a small amount of carbon appears at the surface of the as-deposited films. This carbon layer always appears in an Auger spectrum of as-deposited indium oxide films as a contaminant and comes either from the deposition process or during handling of the films in air after the deposition. In this case, the carbon layer was not thicker than about 8 nm and removed completely after about 5 min of sputtering, resulting in a large increase in the transition intensities of indium and oxygen, as seen in Fig.9b.

Auger depth profiling analysis was carried out on films with thickness from 120 to 1600 nm. All films exhibited an extremely good indepth uniformity, regardless of their thickness, all the way to the interface with the glass substrate. The depth profiles are displayed in two ways. The Auger peak-to-peak signals of indium and oxygen are presented graphically versus sputter depth. By presenting the data in this way it is allowed to compare the trends at indium and oxygen in the same film. Alternatively, the Auger spectra of indium and oxygen collected during a depth profile are shown in a montage plot. Displaying the data in this way allows to establish possible variations, both of peak intensity and position. Fig.10 shows the Auger peak-to-peak signals versus sputter depth for three films with thickness 120, 900 and 1600 nm. The data in Fig.10 were normalized with respect to the reflected electron current. It is striking that even for a 1600 nm thick film the composition stability with depth is comparable to that of the thinner films. The sharp decrease of the oxygen peak-to-peak signal in Fig.10 identifies the interface between film and glass substrate. Fig.11 shows, in a montage plot, all of the Auger spectra of indium and oxygen collected during a depth profile from a given analysed area for a film with thick-

Table 1. Lattice spacings d_{hkl} values as determined for our InO_x films from electron diffraction data and comparison with the corresponding d_{hkl} values of the ASTM diffraction data card 6-0416 for standard In_3O_2 powder.

ASTM 6-0416			Calculated data from TEM	
d(Å)	I/I_0	*hkl*	*D*mm	*d*(Å)
4.13	14	211	55	4.05
2.92	100	222	77	2.89
2.7	2	321		
2.53	30	400	89.5	2.49
2.39	8	411	94.5	2.36
2.26	2	420		
2.16	6	332	104.5	2.13
2.07	2	422		
1.98	10	431	114	1.95
1.85	4	521		
1.79	35	440	126.5	1.76
1.74	4	530		
1.69	2	600		
1.64	6	611	137.5	1.62
1.6	2	620		
1.56	4	541		
1.53	25	622	148.5	1.50
1.46	6	631		
1.46	6	444		
1.43	2	243		

ness 400 nm. The data in Fig.11 were normalized to 1 μA electron current. The shift in the oxygen peak energy position at the interface between film and glass substrate observed in Fig.11, as well as a change in the oxygen peak shape and height, is a clear indication that the bonding configuration of oxygen is changing at the interface from InO_x to SiO_x.

Quantitative Auger analysis was carried out to determine the atomic concentration of indium and oxygen in the films. The method used is based on the simple calculation of relative sensitivities between the elements of interest, indium and oxygen, and silver, from the handbook of standard Auger spectra [36]. All details of the application of this method to our films can be found in a previous work [37]. The fact that the depth profiles exhibited a constant ratio of In to O in the oxide bulk, independently of the thickness, allowed the use of this method for the calculation of the atomic concentrations of In and O throughout the whole thickness of the film, i.e. for each newly exposed surface after a sputter cycle. Fig. 12 shows the atomic concentrations of In and O versus sputter depth for two InO_x films with thickness 440 and 1600 nm deposited with F=0.4 and 1.0 respectively. It is obvious from Fig. 12 that the atomic concentration is constant

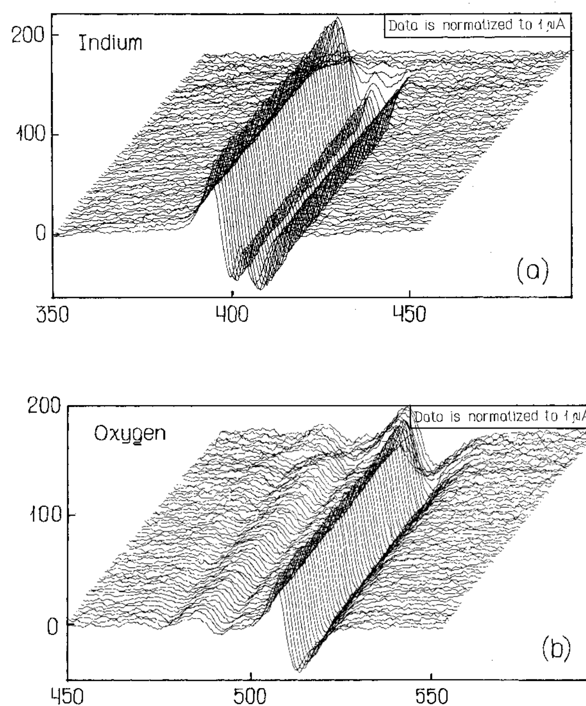

Fig. 11 (a)–(b). Montage plot of the Auger spectra collected during a depth profile of 400 nm thick InO_x film. (a) Indium Auger peaks, (b) Oxygen Auger peaks.

with depth. Similar results with that of Fig. 12 were found for all of the films, independently of thickness and oxygen content during the deposition. The uniformity of the atomic concentration throughout the bulk of the oxide allowed the calculation of an average atomic concentration of In and O in each film from the values of the atomic concentration in different depths during a depth profile. This way of presenting the results was convenient for a better comparison between the different films. Table 2 shows the average atomic concentration of some representative InO_x films prepared with various thicknesses in various mixtures of oxygen in argon during the deposition. The atomic ratios of oxygen to indium listed in Table 2 should be compared to 1.5 for the stoichiometric In_2O_3. From Table 2 it appears that there is an oxygen deficiency of about 2-5% in the InO_x films compared to stoichiometric In_2O_3 (60% at. Oxygen and 40% at. Indium). This is in good agreement with previously reported values [29] of oxygen/metal atomic ratios calculated from the surface of indium oxide films by quantitative Auger analysis using a standard In_2O_3 sample with a known composition. Deviations from stoichiometry up to a maximum of about 10% from one sample to the other have been reported by other researchers [11] using the technique of energy dispersive x-ray analysis. The quantitative Auger analysis presented here gave an oxygen concentration which varies from $O_{2.75}$ to $O_{2.90}$ for the examined films. This is in good agreement with the result $O_{2.92\pm0.03}$ obtained from high accuracy

Table 2. Average atomic concentration of In and O in InO_x films as determined by AES quantitative analysis.

Oxygen volume fraction, F	Thickness (nm)	Average at.% In	Averege at.% O	Atomic ratio O/In
0.4	440	46	54	1.2
0.5	600	46	54	1.2
0.6	1200	44	56	1.3
0.8	900	43	57	1.3
1.0	1600	42	58	1.4

wavelength dispersive x-ray analysis (WDX) carried out by Bellingham et al. [21] on InO_x films with a thickness of 700 nm produced by ion beam sputtering.

Quantitative analysis with reference to standard In_2O_3 powder of known concentration has been carried out on InO_x films by using the energy dispersive x-ray analysis technique, in which the sample is bombarded by an electron beam, causing the emission of characteristic x-rays. In this case, the quantitative analysis was carried out through comparison of the EDX spectra of the films with that from the standard In_2O_3 being in the form of fine grained powder. This method was applied to determine the average stoichiometry of as-deposited InO_x films produced in various mixtures of oxygen in argon during the deposition onto silicon substrates. Fig. 13 shows the EDX spectra of the standard and a microcrystalline InO_x film with thickness of 600 nm deposited with $F = 0.5$ onto glass substrate. The spectrum in Fig. 13 was made with an acceleration voltage of 5.5 kV. This voltage was carefully chosen (details are available in a previous work [37]) to avoid excitation of oxygen in the glass substrate and to make sure that all the x-ray producing volume would be inside the film. For the best accuracy, the standard was mounted in the system along with the sample examined. In this way, the spectra of the standard and the InO_x film were taken under the same conditions, i.e. same acceleration voltage, incident angle, detector settings etc. In the EDX quantitative analysis carried out on the InO_x films deposited onto silicon substrates, the standard was analysed two times and the average result was used for the comparison. Also in this case, the samples of interest were mounted in the system along with the standard sample. Table 3 shows the results of the EDX quantitative analysis for InO_x films prepared under the same deposition conditions with those in Table 2. It is seen from the Table 3, that the as-deposited InO_x films seem to consist of 71-72 at. % oxygen, which would be 11-12 at. % more than the stoichiometric composition. This is not in agreement with the results of the quantitative Auger analysis given above. The reason for this discrepancy is clearly that the standard was in the form of powder with grains in the micron range, while the films have very smooth surfaces and grains of the size of 20.6 nm. This makes the surface of the powder appear as a very rough system compared to that of the InO_x films. For the indium x-ray signal with an energy of 3.3 keV this is not so critical, but for the oxygen x-rays with an energy of only 0.525 keV it becomes a significant disturbance. The oxygen K_α x-rays are strongly absorbed by the indium atoms, so a surface roughness causes variations in the path length of x-rays emerging from the sample, resulting in a larger absorption of the oxygen x-rays. This effect has also been observed by Bellingham et al. [21]. The effect is also confirmed by the fact that the indium signal has about the same intensity in the samples as in the standard, whereas the oxygen signal is strongly reduced in the standard, as

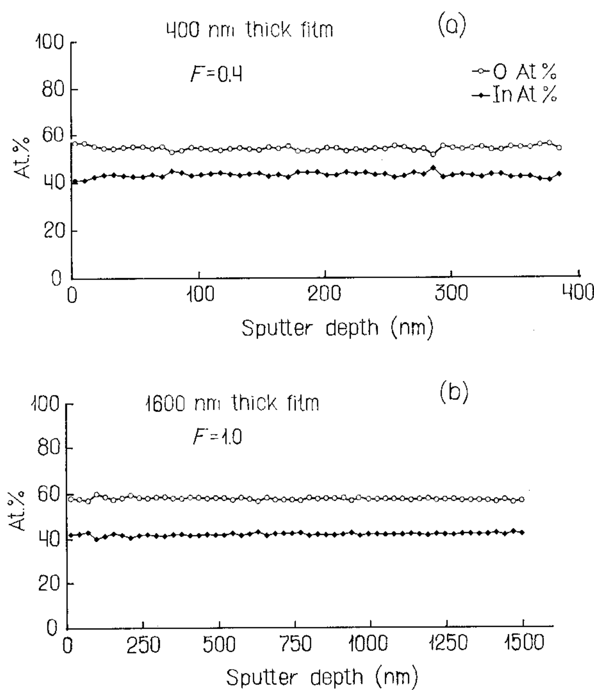

Fig. 12 (a)–(b). Atomic concentrations of In and O versus sputter depth of 440 and 1600 nm thick InO_x films produced in a plasma having an oxygen fraction of (a) F=0.4 and (b) F=1.0, respectively.

Table 3. Average atomic concentration of In and O in InO_x films as determined by EDX quantitative analysis.

Oxygen volume fraction, *F*	Thickness (nm)	Average at.% In	Avereg at.% O
0.4	440	29.0	71.0
0.5	600	29.0	71.0
0.6	1200	28.5	71.5
0.8	900	28.1	71.9
1.0	1600	29.4	70.6

shown in Fig. 13. The only way to obtain a reliable EDX analysis of an InO_x film is by using a standard with the same roughness as the film. This was not available for the measurements. Nevertheless, the results are important in the sence that all films exhibited the same stoichiometry, independently of the oxygen content used during growth, and from this point of view the EDX results are in perfect agreement with those of AES analysis.

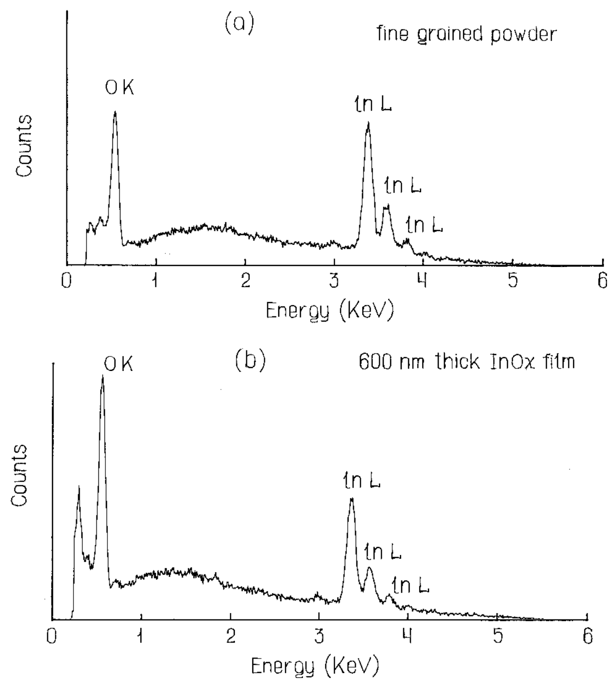

Fig. 13 (a)-(b). EDX spectra of (a) the standard In_3O_2 in the form of fine-grained powder and (b) 600 nm thick as-deposited microcrystalline InO_x film onto Corning 7059 glass substrate.

Photorefractive properties. A typical sequence of holographic grating recording (parts A and B) and decay (part C) in InO_x films is depicted in Fig. 14. A maximum diffraction efficiency of $\eta \sim 10^{-4}$ is observed for a grating recorded in 600-800 nm thick InOx films. In the rising part of the trace all three (recording and probe) beams are present, while the decay is observed in the absence of both recording beams. The HeNe beam is always present to probe the evolution of the grating being recorded. It was observed that the probe beam does not affect the recording characteristics that are solely associated with the UV radiation. No darkening or coloration of the film was observed. Nevertheless the existence of an absorption component of the gratin cannot be excluded.

Illumination with UV light in air increases the conductivity of an InO_x film by two orders of magnitude. Fig. 15 depicts the absolute change of the diffraction efficiency and the conductivity of InO_x film upon illumination with an HeCd laser beam of intensity I=40 mW/cm^2. The new electrical state of the film is maintained until the film is exposed to an ozone atmosphere. It is noted that with the 50 Ω termination at the oscilloscope we were restricted in monitoring only the high current values, thus enabling us to observe only the high conductivity levels, which correspond to saturation. The similarity of the two curves and the correspondence of the two phenomena are apparent indicating a direct relation between conducting state and recording efficiency. A rapid rise of the diffraction efficiency is related to the increase in conductivity while the dynamics of the decay characteristics are almost the same in both actions. Although the conductivity level remains constant during recording, the diffraction efficiency behavior seems to be affected by two processes. A fast rise occurs immediately after the interference of the recording beams (part A), which is followed by a slight reduction and a stabilization stage (part B). In the absence of ultraviolet radiation both conductivity and diffraction efficiency decay exponentially (part C).

The hologram decay does not follow a simple exponential form. Double exponential decay curves [$\eta = A_1 \exp(-t/\tau_1) + A_2 \exp(-t/\tau_2)$] fit well to the decay data (mean square error 10^{-5}). Time constants of τ_1=6.3 s and τ_2=43.5 s have been extracted from the fitting procedure. The decay time constants remain practically the same for all values of Λ in the range of 0.6-3 μm. This is in contrast with the well-known case of non-localized photorefractive materials involving charge diffusion or drift, verifying the localized nature of the observed effects.

For the permanent holographic recording utilizing UV radiation of 193 nm emitted by an ArF excimer laser, the recording dynamics are depicted in Fig.16 showing the results of a sequence of 9 laser pulses used to achieve saturated grating recording at an energy fluence of 18 mJ/cm^2 per pulse. Corresponding AFM analysis of the illuminated area (Fig. 17) shows a surface relief pattern of periodicity Λ=0.65 μm. The dynamics of the above two processes are discussed in the following.

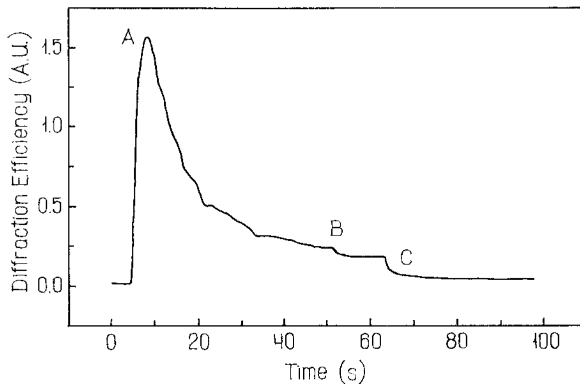

Fig. 14. Typical holographic recording behavior observed in InO_x samples. Decay times were measured in region C. Typical values calculated were τ_1=6.3 sec and τ_2=43.5 sec.

4. DISCUSSION

It has been shown that, under the present deposition conditions, high quality microcrystalline InO_x films have been produced at room temperature. The results presented above demonstrate that the electrical, optical and chemical properties of these films do not depend critically on the growth parameters, i.e. film thickness and oxygen content during the deposition. From this point of view, it becomes clear that reactive dc magnetron sputtering from a pure In target has the advantages of high reproducibility and good control of film properties over other deposition techniques for the preparation of transparent indium oxide films.

Microcrystalline InO_x films with high transparency in the visible light region have been prepared using reactive sputtering of pure In at room temperature. It has been shown that the conductivity of these films can be changed in a controlable and fully reversible manner by about six orders of magnitude by alternately exposing the films to UV light in vacuum and reoxidizing them in an ozone atmosphere. These observations do not depend critically on the preparation conditions. The same results have been essentially found for InO_x films produced with oxygen contents between F = 0.4 and 1.0 in the sputtering gas. The mechanism responsible for these large changes in conductivity is believed to be the UV induced production of oxygen vacancies, which act as doubly charged donors providing electrons to the conduction band. An oxygen vacancy is formed when an oxygen atom in a normal lattice site is removed, which is usually equivalent to a transformation of an oxygen atom in a normal site to the gaseous state. Considering that in binary oxides the oxygen ions in the regular sites have a valency of -2, in this process, the two electrons of the oxygen ion are left in the vacant site. If both of these two electrons are localized at the oxygen vacancy,

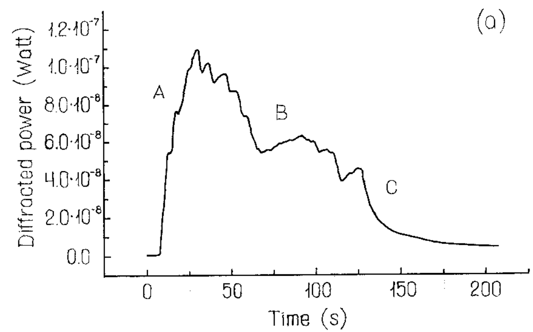

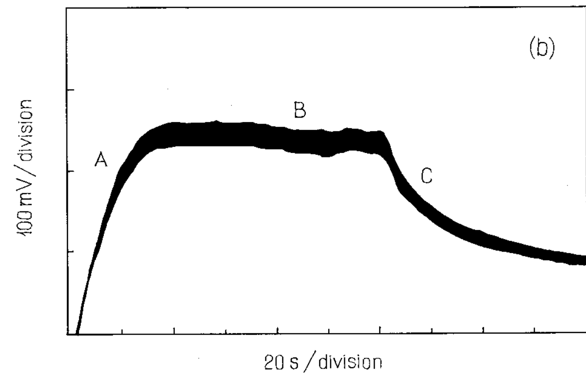

Fig. 15 (a)-(b). Simultaneous recording of: (a) the dynamics of the holographic grating and (b) conductivity.

charge neutrality is preserved and the oxygen vacancy has zero effective charge. If one or both of the localized electrons are excited and transferred away from the vacancy, the oxygen vacancy becomes singly or doubly ionized, respectively. Since electrons are removed, the ionized oxygen vacancy will have an effective positive charge to conserve the electrical neutrality of the material. The charged oxygen vacancy becomes an electron trapping site but in this process one or two electrons are available for conduction. The process of formation of doubly charged oxygen vacancies can be described by the following defect equation [38]:

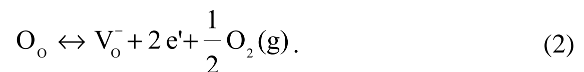

$$O_o \leftrightarrow V_o^{\cdot\cdot} + 2\,e' + \frac{1}{2}O_2(g)\,. \qquad (2)$$

From Eq. 2 it arises that the presence of oxygen vacancies is equivalent to the existence of oxygen deficiency with respect to the stoichiometric composition. Therefore, the large conductivity changes observed in the films under UV photoreduction result directly from a deviation in the stoichiometry of these films. The formation of charged oxygen vacancies lead to the formation of complimentary free electrons. During photoreduction, a large increase in the free electron concentration occurs due to the increase in the number of charged oxygen vacancies. Subsequently, during oxidation, the incorporation of oxygen leads to annihilation of the charged oxygen vacancies, and

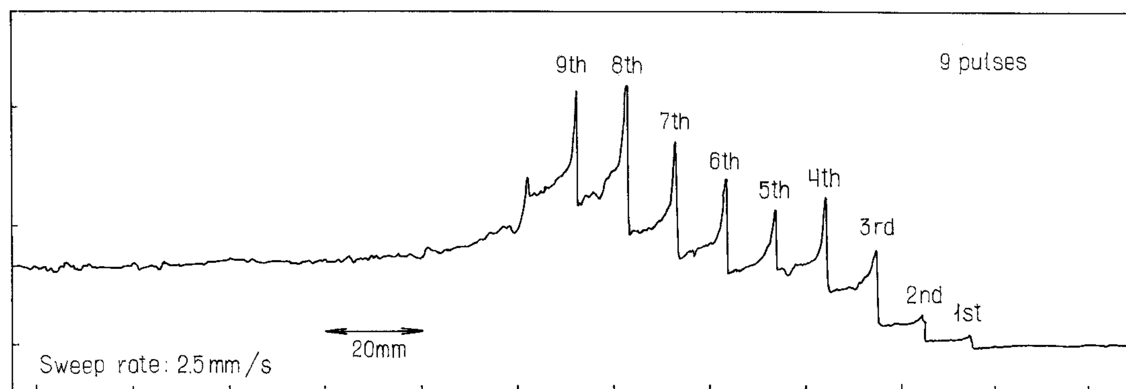

Fig. 16. Chart recorder traces of the diffracted signal, showing the dynamics of recording and decay of a grating in sputtered indium oxide film grown under 50%O_2/50%Ar pressures, 9 consecutive pulses were used to achieve saturation.

hence to a drastic fall in the free electron concentration. For the polycrystalline films it is visualized that oxygen produces a state below the conduction band, which removes one electron from the conduction band for each oxygen chemisorbed. Since indium oxide is an n-type semiconductor, the effect of oxygen diffusion is to decrease the dark conductivity. When an oxygen vacancy is initially formed, the chemical bonds of an oxygen atom to the neighboring atoms are broken. Therefore, it is expected that the process of formation of an oxygen vacancy is related to the oxygen bond strength in the oxide. From this point of view, indium oxide is considered as a chemically relatively unstable material, so that it is relatively easy to be reduced and oxidized.

All the investigated samples were microcrystalline with a grain size between 10 nm (detection limit) and 100 nm. With increasing temperature the roughness increases only slightly while the grain size remains nearly constant. InO_x layers on corning glass with different layer thickness (i.e. different sputtering times) at otherwise constant growth conditions were examined. A perculated layer with a distinct grain structure was already found for the thinnest layers (10 nm). The grain size as estimated by XRD corresponds well to the layer thickness, while the lateral grain size by AFM is exceeding this value. With progressing deposition this grain size drops down to a minimum after which it is increasing monotonically with the layer thickness. In contrary, on silicon substrates the grain size was increasing all over the investigated range. Thus the nucleation of the InO_x layers is strongly affected by the roughness of the substrate. At layer thicknesses exceeding 200 nm the grains are starting to aggregate to clusters. As expected the surface roughness is increasing monotonically with progressing deposition time. The scaling exponent for the surface roughness (0.55) is in good agreement with theoretical descriptions for "random deposition" [39].

The sensitivity of the conductivity of InO_x on a reactive gas environment shows its potential as a thin film gas sensor. However, the detection of gases using thin film sensors requires an interaction with the surface of the thin active layer. Therefore structure and effective surface area of this layer are expected to have an influence on the sensitivity. Moreover the grain size is known to dictate the conductivity of polycrystalline materials. Thus the knowledge and the control of the grain size and the surface morphology is an important factor for a better understanding of the detection mechanism of oxidizing gases and the optimization of a sensor device.

The TEM studies carried out on InO_x films with a thickness of about 100 nm showed that the films consisted of a large area of intergranular amorphous phase. *In situ* electron beam recrystallization was observed to take place in these films. This effect was also observed by Rauf [40] for indium oxide films prepared with the reactive thermal evaporation technique. The electron diffraction pattern of the as-deposited InO_x

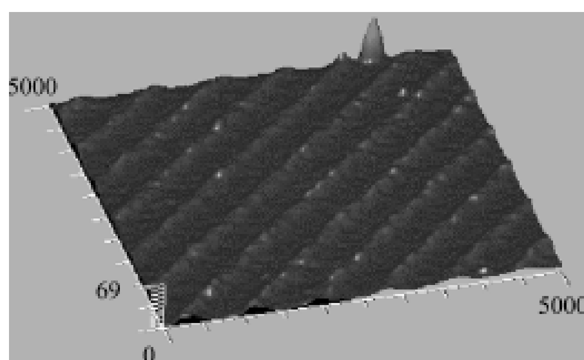

Fig. 17. AFM scans of the illuminated area revealing a surface relief pattern of periodicity Λ=0.65MM.

films consisted mainly of diffuse rings with only a few crystallites embedded in the uniform matrix. This was due to the small thickness of the film (of about 100 nm). The same selected area of the film after about 10 min of irradiation with the focused electron beam exhibited an electron diffraction pattern consisting of sharp diffraction rings, typical of a microcrystalline In_2O_3 film. This means that the initial amorphous phase crystallized around the already present crystallites. This can be interpreted as a rapid growth of initial neighboring crystallites to new, highly ordered crystallites by electron beam induced annealing. Rauf, using a high-resolution JEOL 2000EX transmission electron microscope, observed that indium oxide films containing both amorphous and crystalline phases are usually highly disordered. Even crystalline grains observed in these films seemed to have high defect densities. These defects include stacking faults, dislocations, impurity atoms and oxygen vacancies. The electron beam irradiation brings the amorphous phase in a higher-energy state so that the ordering process in this region is very fast. Rapid growth of the originally existing neighboring crystallites occurs forming highly ordered recrystallized crystallites into the amorphous phase, by annealing the defects out to the boundaries separating these crystallites. By migration of defects toward grain boundaries the material has a tendency to crystallize around the initially formed highly ordered crystallites. Kasiviswanathan and Rangarajan [41] have produced indium oxide films with a thickness of 70 nm by dc reactive magnetron sputtering in the presence of pure oxygen at room temperature and observed that the as-deposited films exhibited a clear microcrystalline structure which was evident by the well defined rings in the electron diffraction patterns. This probably results from the fact that the growth of these films occured in a pure oxygen atmosphere, since the films prepared in the present work with a thickness of about 100 nm in a mixture of argon-oxygen plasma were found to be mainly amorphous in their as-deposited state. The existence of more oxygen in the plasma may lead to a faster chemical reaction with the available In bonds at the first stage of the deposition process and therefore to a faster growth of In_2O_3 crystallites. A crystallite size of 20 nm was reported, also by Kasiviswanathan and Rangarajan, for dc sputtered indium oxide films. The lattice spacings d_{hkl} values calculated for the InO_x films in the present work differs by about 1% from the corresponding ones of the ASTM standard In_2O_3 powder. Similar variation of about 1% from the standard values has also been found by Kasiviswanathan and Rangarajan by applying the relativistic correction for the calculation of the de Broglie wavelength from the accelerating potential. It should also be noted that the crystal planes (400), (411) and (611), which are absent in the x-ray diffraction pattern of the as-deposited microcrystalline InO_x films, clearly appear in the electron diffraction pattern of thinner films ($d \leq 100$ nm) after crystallization occured. This is because very few grains are oriented in these directions. As seen from the electron diffraction pattern, the reflections from individual grains can be recognized as separate spots in the diffraction rings of these planes, whereas the reflections from the preferred orientation planes like (222) and others, are so numerous that they make up continuous rings.

The Auger depth profiling analysis showed that the composition of the InO_x films remains constant all the way from the surface down to the interface with the glass substrate, regardless of the thickness of the films. Even for films with thickness of 900, 1200 and 1600 nm, the depth profiles are comparable to those of the thinner films. This shows that the growth process itself is extremely well controlled to produce films with high homogeneity at room temperature. The quantitative AES and EDX analyses were carried out on batches of films produced in the same sputtering deposition runs. Both AES and EDX analyses have confirmed that the composition of the films is invariant for a variation of the oxygen volume fraction between $F = 0.4$ and 1.0 in the growth plasma. However, the results of the AES analysis indicate the existence of an oxygen deficiency of 2-5 % in the films with respect to the stoichiometric composition, while those of the EDX analysis seemed initially to indicate an oxygen excess (metal deficiency) of 11-12% with respect to the stoichiometric composition. This discrepancy was attributed to the roughness of the standard material used in the EDX analysis, compared to the very smooth surface of the films. Because of this roughness, which is significant compared to the depth of x-ray production in the standard, the oxygen signal of the standard appeared strongly reduced compared to the oxygen signal from the sample. For this reason, the EDX analysis was not able to provide the correct stoichiometry in the case of these films. However, the accuracy of the method itself is evaluated in terms of providing a very good compositional comparison between the films. All of the films produced with oxygen contents between $F = 0.4$ and 1.0 in the sputtering gas exhibited essentially the same stoichiometry (~71% O, ~29 % In). This means that even at an oxygen concentration of $F = 0.4$ there is enough oxygen in the plasma to react with the available In bonds to transform the material from a metallic into a semiconducting/insulating transparent state. This, in turn, is an evidence that the excess oxygen in the deposition plasma does not contribute to the chemical composition of the film but merely to the sput-

tering rate. The deviation of 2-5 % from the stoichiometric composition as consistently revealed by the present AES analysis, is in good agreement with previously reported results from Auger quantitative analysis and comparable with those of EDX and WDX analysis carried out by other researchers. Therefore, the above AES results can be safely used as an absolute measurement of composition for the InO_x films.

Since InO_x in its slightly non-stoichiometric form discussed above is a material that contains significant amount of localized centers with trapped electrons, it is a candidate behaving as other well know photorefractive materials for which the trapped electrons may be excited by light of an appropriate wavelength. It was this property of InO_x that was exploited during the present study. Thus two coherent beams of light (the writing beams) interfering in the InO_x films caused the excitement of electrons from the traps to the conduction band at rates proportional to the light intensity at any given point. Subsequently this gives rise to an inhomogeneous concentration of free electrons that drift and diffuse away from the region of high-intensity light (interference maxima) and are collected (trapped) in regions of low-intensity light (interference minima). As a result it is noticed a net accumulation of a negative and positive space charge in regions exhibiting a sinusoidal interference pattern with a corresponding strong spatially periodic electric field. This dc field causes the deformation of the crystal lattice leading to a refractive index modulation and the subsequent production of a phase hologram.

A possible explanation of the origin of the observed behavior may involve active centers, such as oxygen vacancies, related to the growth conditions and specific nature of the material. These localized states can be altered by UV radiation and their decay to the initial condition is associated with characteristic time constants that depend on the specific nature of the active centers and the material. It is noted here that holographic recording measurements were performed with a large variety of specimens. Even though they were grown during different runs of the sputtering machine, they all exhibited identical temporal behavior under the same experimental conditions.

The dynamics of the recording and decay can be understood in terms of coexistence of two different types of non shifted gratings within the material. The first corresponds to UV induced electrical conductivity changes, exhibits unusually large coupling strengths and a dynamic behavior associated with localized modification of the optical properties of the material and a thermal decay of the conductivity grating. This behavior is as stated above, attributed to the existence of active centers in the material and associates with the presence of oxygen vacancies in the film lattice. The second is attributed to structural gratings, which remain after the thermal decay of the conductivity grating. The interpretation of the results are in line with the model of Szorenyi et al [42], in which excimer laser radiation causes changes of optical properties of ITO films by melting and resolidification processes for fluences below the ablation threshold. Thus we attribute this stable grating recording to spatial periodic modifications of the concentration of defects induced by the interference of the intense UV radiation.

5. CONCLUSIONS

InO_x thin films deposited by dc sputtering show novel sensor and optoelectronic properties. They exhibit high reversible conductivity changes, in the range of six orders of magnitude, caused by photoreduction in UV light and subsequent oxidation in ozone atmosphere. Consequently, InO_x thin films can potentially be applied as ozone sensors. Their sensitivity to ozone is dependent on their thickness. It decreases smoothly with increasing film thickness. The crystallinity and microstucture of InO_x thin films are greatly dependent on the substrate temperature as well as on the film thickness. An amorphous to polycrystalline transition occurs by increasing substrate temperature and film thickness. InO_x films prepared by dc sputtering exhibit good in-depth uniformity regardless of their film thickness in the range of 120-1600 nm. An oxygen deficiency of 2-5% has been observed with respect to the stoichiometric composition. Finally, permanent holographic recording has been realized in thin films using UV radiation at 193 nm emitted by an ArF excimer laser. The photorefractive properties of InO_x films are very promising for novel telecom and waveguide applications.

ACKNOWLEDGEMENTS

The authors would like to thank their partners at the Optoelectronics Research Centre, Southampton University, UK, the Department of Physics, Odense University, Denmark and finally the Laser Division at FORTH/IESL, Greece for their fruitful scientific cooperation.

REFERENCES

[1] C.E. Wickersham and J.E. Greene // *Phys. Stat. Sol. (a)* **47** (1978) 329.

[2] T. Suzuki, T. Yamazaki, M. Takizawa and O. Kawasaki // *J. Mat. Sci.* **24** (1989) 187.

[3] A.N.H. Alajili and S.C. Bayliss // *Thin Solid Films* **305** (1997) 116.

[4] C.A. Pan and T.P. Ma // *J. Electrochem. Soc.* **128** (1981) 1953.

[5] S. Muranaka, Y. Bando and T. Takada // *Thin Solid Films* **151** (1987) 355.

[6] S. Naseem, I.A. Rauf, K. Hussain and N.A. Malik // *Thin Solid Films* **156** (1988) 161.

[7] V. Korobov, M. Leibovitch and Y. Shapira // *Appl. Phys. Lett.* **65** (1994) 2290.

[8] P. Thilakau and J. Kumar // *Thin Solid Films* **292** (1997) 50.

[9] K.G. Copchandran, B. Joseph, J.T. Abraham, P. Koshy and V.K. Vaidyan // *Vacuum* **48** (1997) 547.

[10] K.B. Sundaram and G.K. Bhagavat // *Phys. Stat. Sol. (a)* **63**, (1981) K15.

[11] V. Damodara Das, S. Kirupavathy, L. Damodare and N. Lakshminarayan // *J. Appl. Phys.* **79** (1996) 8521.

[12] A.P. Mammana, E.S. Braga, I. Torriani and R.P. Anderson // *Thin Solid Films* **85** (1981) 355.

[13] J.C. Manifacier, L. Szepessy, J.F. Bresse, M. Perotin and R. Stuck // *Mat. Res. Bull.* **14** (1979) 163.

[14] W. Siefert // *Thin Solid Films* **120** (1984) 275.

[15] S. Mailis, C. Grivas, D. Gill, L. Boutsikaris, N.A. Vainos, C. Xirouchaki, G. Vasiliou, N. Garawal, G. Kiriakidis and H. Fritzsche // *Optical Memory and Neural Networks* **5** (1996) 191.

[16] B. Pashmakov, B. Claflin and H. Fritzsche // *Solid State Commun.* **86** (1993) 619.

[17] B. Pashmakov, H. Fritzsche and B. Claflin // *J. Non-Cryst. Solids* **441** (1993) 164.

[18] H. Fritzsche, B. Pashmakov and B. Claflin // *Sol. Energy Mater. Solar Cells* **32** (1994) 383.

[19] B. Claflin and H. Fritzsche // *J. Electr. Mater.* **25** (1996) 1772.

[20] C. Xirouchaki, G. Kiriakidis, T.F. Pedersen and H. Fritzsche // *J. Appl. Phys.* **79** (1996) 9349.

[21] J. R. Bellingham, A.P. Machenzie and W.A. Philips // *Appl. Phys. Lett.* **58** (1991) 2506.

[22] K. Ito, T. Nakazawa and K. Osaki // *Thin Solid Films* **151** (1987) 215.

[23] C.H. Lee, C.V. Kuo and C.L. Lee // *Thin Solid Films* **173** (1989) 59.

[24] N.R. Armstrong, A.W.C. Lin, M. Fujihira and T. Kuwana // *Anal. Chem.* **48** (1976) 741.

[25] A. W.C. Lin, N.R. Armstrong and T. Kuwana // *Anal. Chem.* **49** (1977) 1228.

[26] L.L. Kazmerski, P.J. Ireland, P. Sheldon, T.L. Chu, S.S. Chu and C. Lin // *J. Vac. Sci. Technol.* **17** (1980) 1061.

[27] J.C.C. Fan and J.B. Goodenough // *J. Appl. Phys.* **48** (1977) 3524.

[28] A. Golan, J. Bregman, Y. Shapira and M. Eizenberg // *J. Appl. Phys.* **69** (1991) 1494.

[29] J.I. Jeong, J.H. Moon, J.H. Hong, J.S. Kang, Y. Fukuda and Y.P. Lee // *J. Vac. Sci. Technol. A* **14** (1996) 293.

[30] V.D. Das, S. Kirupavathy, L. Damodare and N. Lakshminarayan // *J. Appl. Phys.* **79** (1996) 8521.

[31] B.M. Kostishko, A.M. Orlov and L.I. Gonchar // *Inorg. Mater.* **33** (1997) 816.

[32] S. Mailis, L. Boutsikaris, N.A. Vainos, C. Xirouhaki, G. Vasiliou, N. Garawal, G. Kiriakidis and H. Fritzsche // *Appl. Phys. Lett.* **69** (1996) 2459.

[33] K. Moschovis, E. Gagaoudakis, E. Chatzitheodoridis, G. Kiriakidis, S. Mailis, E. Tzamali, N.A. Vainos and H. Fritzsche // *Appl. Phys. A* **66** (1998) 651.

[34] S. Pissadakis, S. Mailis, L. Reekie, J. S. Wilkinson, R. W. Eason, N.A. Vainos, K. Moschovis and G. Kiriakidis // *Appl. Phys. A* **69** (1999) 333.

[35] J. A. Thornton // *J. Vac. Sci. Technol. A* **4** (1976) 3059.

[36] P.W. Palmberg, G.E. Riach, R.E. Weber and N.C. MacDonald, *Handbook of Auger Electron Spectroscopy* (Physical Electronics Industries, Minesota, 1972).

[37] C. Xirouchaki, K. Moschovis, E. Chatzitheodoridis, G. Kiriakidis and P. Morgen // *Appl. Phys. A* **67** (1998) 295.

[38] P. Kofstad, *Non-stoichiometry, Diffusion and Electrical Conductivity in Binary Metal Oxides* (Wiley, U.S.A., 1972).

[39] Barabasi and H.E. Stanley, *Fractal concepts in Surface Growth* (Cambridge University Press, Cambridge, 1995).

[40] I.A. Rauf // *J. Appl. Phys.* **79** (1996) 4057.

[41] S. Kasiviswanathan and G. Rangarajan // *J. Appl. Phys.* **75** (1994) 2572.

[42] T. Szorenyi, L. D. Laude, I. Bertoti, Z. Kantor and Zs. Geretovsky // *J. Appl. Phys.* **78** (1995) 6211.